Supporting Information

Nanomechanics of Anion-π Interaction in Aqueous Solution

Jiawen Zhang,[†,⊥] Li Xiang,[†,⊥] Bin Yan,[†,‡] and Hongbo Zeng*[,†].

[†]Department of Chemical and Materials Engineering, University of Alberta, Edmonton, Alberta, T6G 1H9, Canada
[‡]College of Light Industry, Textile & Food Engineering, Sichuan University, Chengdu, Sichuan, 610065, China

1. Materials and synthesis

1.1 Materials

2,3-Dihydroxybenzoic acid (2,3-DHBA), benzyl bromide (BnBr), potassium hydroxide (KOH), N,N′-dicyclohexylcarbodiimide (DCC), O-phosphorylethanolamine (O-PEA), Pd/C, dimethyl sulfoxide (DMSO), N-hydroxysuccinimide (NHS), potassium bicarbonate ($KHCO_3$), bicine, tetrahydrofuran (THF), methanol (MeOH) and 1,4-cyclohexadiene were purchased from Sigma-Aldrich. Methylene chloride (DCM) was purchased from Fisher Scientific, Canada. All chemicals were used as received without further purification.

1.2 Synthesis of 2,3-dibenzyloxy-benzoic acid (2,3-2Bn-BA) from 2,3-DHBA

The synthesis was based on a previous report.[1] 2,3-DHBA (2 g) and powdered KOH (10.28 g) were dissolved into DMSO (40 mL). Followed by addition of benzyl bromide (6 mL), the mixture was allowed to react overnight under stirring. Then the product was obtained and purified by extraction (EtOAc) and rotary evaporation. 1H NMR spectrum (d_6-DMSO, 400 MHz): δ 7.51-7.09 (m, 13 H; Ph) δ 5.17 (s, 2H; O=CPhOC**H₂**) δ 4.99 (s, 2H; PhOC**H₂**).

1.3 Synthesis of 2-O-phosphorylethanol 2,3-dibenzyloxy-benzamide (PO_4-2Bn-B)

The synthesis was performed according to a previously reported method.[2] 2,3-2Bn-BA (2 g) and NHS (0.72 g) was dissolved in 40 mL of THF in a round-bottom flask with ice bath cooling, followed by the dropwise addition of DCC (1.30 g) in THF (10 mL). The reaction was monitored by TLC and the resulted mixture was filtered. The filtrate was concentrated and purified by column chromatography. 1H NMR spectrum (d_6-DMSO, 400 MHz) of the resulted product, 2,3-dibenzyloxy-benzoic acid NHS ester (2,3-2Bn-BA-NHS): δ 7.64-7.18 (m, 13H; Ph) δ 5.23 (s, 2H; O=CPhOC**H₂**) δ 5.03 (s, 2H; PhOC**H₂**) δ 2.87 (s, 4H; NO=CC**H₂**). 2.4 g of 2,3-2Bn-BA-NHS was weighed and dissolved in 10 mL THF, and then dropped to a mixture of O-PEA (2.62 g) and $NaHCO_3$ (4.15 g) in 60 mL of 50% aq. THF. The reaction was monitored by TLC. Followed by aqueous work-up (CH_2Cl_2), the product was purified by column chromatography. 1H NMR spectrum (d_6-DMSO, 400 MHz): δ 8.30 (t, J=5.7 Hz, 1H; N**H**) δ

7.61-6.98 (m, 13 H; Ph) δ 5.18 (s, 2H; O=CPhOC**H₂**) δ 5.01 (s, 2H; PhOC**H₂**) δ 3.86 (t, J=6.2 Hz, 2H; OC**H₂**CH_2) δ 3.41 (t, J=6.0 Hz, 2H; NHC**H₂**).

1.4 Synthesis of 2-O-phosphorylethanol 2,3-hydroxybenzamide (PO_4-DHB)

The removal of benzyl protect group (Bn) was achieved based on a previous report.[3] 700 mg of PO_4-2Bn-B was dissolved in MeOH. Then 700 mg of 10% Pd/C solution in 5 mL of DCM was dropped into the previous mixture, followed by the dropwise addition of 4 mL 1,4-cyclohexadiene under Argon atmosphere. The reaction was allowed to react for 5 hrs. Then the mixture was filtrated and evaporated to obtain the final product. 1H NMR spectrum (d_6-DMSO, 400 MHz): δ 8.97 (t, J=5.4 Hz, 1H; N**H**) δ 7.28-6.67 (m, 3H; Ph) δ 3.95 (t, J=5.8 Hz, 2H; OC**H₂**) δ 3.49 (t, J=5.7 Hz, 2H; NHC**H₂**).

2. Methods and characterizations

2.1 Surface force measurement

The normal force-distance profiles and adhesion forces of poly(PO_4-DHB) coatings under various aqueous conditions were determined using a surface forces apparatus (SFA) in a configuration reported previously.[4-6] Briefly, two back-silvered mica sheets glued on the cylindrical silica disks (radius R = 2 cm) were mounted in the SFA chamber in a cross-cylinder configuration, which is locally equivalent to a sphere of radius R against a flat surface at a separation distance of $D \ll R$. During the SFA force measurement, D was obtained by monitoring the optical interference fringes of equal chromatic order (FECO) based on the multiple beam interferometry (MBI) optical technique, and the interaction forces were calculated through the deflection of the cantilever spring using Hooke's law. The reference distance ($D_0 = 0$) was determined from an independent measurement of the contact point at which two bare mica surfaces were contacted in air. The adhesion energy per unit area (W_{ad}) was deduced from the measured adhesion force (F_{ad}) based on the Johnson−Kendall−Roberts (JKR) model where $W_{ad}=F_{ad}/1.5\pi R$.[7-8]

For the force measurement during the deposition process, a droplet of 100 μL as-prepared PO_4-DHB buffer solution, with existence of different kinds of salt ions, was injected between two mica surfaces, to study the influence of salt ion types on the interaction behavior and deposition capability. The interaction forces were measured with the variation of deposition time. During a typical force measurement, two surfaces were firstly brought together to reach a “hard wall” and kept in contact for a certain time before the separation. The “hard wall” distance was defined as the formed coating thickness, which did not significantly vary with the increase of normal load. For the force measurement between two as-formed poly(PO_4-DHB) coatings, the coatings were firstly deposited on mica surfaces, and then the two surfaces were transferred to the SFA chamber. The effect of salt species and salt

concentrations on the interaction forces was studied by injecting a droplet of 100 μL buffer solution containing different salt ions and salt concentrations between two transferred surfaces followed by the same force measurement method as described above.

2.2 Quantum simulation

The density function theory simulation was performed using Gaussian 09 program package.[9] All the calculations were performed at b3lyp/6-311+g(d,p) level with D3BJ dispersion and zero-point vibrational correction, and SMD (water) implicit solvation model was used.[10] For simplicity, the methyl amide of catechol, quinone and *o*-semiquinone radical, denoted as CMA, QMA, QRMA respectively, was used as the model π-conjugated systems, and methyl phosphate was used as the model anionic phosphate ester. The optimized geometries of methyl phosphate ($MePO_4^{2-}$)-CMA/QMA/QRMA-K^+ were obtained. The electrostatic potential (ESP) surfaces of optimized CMA/QMA/QRMA-K^+ pairs, and the binding energies between $MePO_4^{2-}$ and each CMA/QMA/QRMA-K^+ pairs were computed. The optimized geometries of NO_3^-/HPO_4^{2-}/SO_4^{2-}-QMA-K^+ were also simulated, and the binding energy between NO_3^-/HPO_4^{2-}/SO_4^{2-} and QMA-K^+ pairs were obtained. All the stability of optimized geometry was verified by vibrational analysis. The binding interaction energy was defined as: Binding energy = $E_{complex} - (E_{anion} + E_{pair})$, where $E_{complex}$, E_{anion} and E_{pair} are the total ground state energies of each type of complex, anion and pair in water, respectively.

2.3 Time-of-flight secondary ion mass spectrometry (ToF-SIMS) characterization

The composition characterizations of mica and poly(PO_4-DHB) coated mica surfaces were performed by ToF-SIMS analysis in negative-ion mode using an TOF.SIMS 5 instrument (IONTOF GmbH, Münster, Germany) with a 25 keV Bi^+ primary ion source. The primary Bi^+ ion beam was operated at 19 ns with ~1 pA pulsed beam current. The mass anaysis was carried out by using a Time of Flight analyzer and the mass scale was calibrated using H^-, C^-, and O^- peaks. As shown in Figure S2a), the abundant characteristic ions on mica included C_2H^-, Cl^-, SiO_2^- and SiO_3^-.With the poly(PO_4-DHB) coating on mica surface, as shown in Figure 2b), the characteristic ion peaks of the poly(PO_4-DHB) coating emerged, including NC^-, NCO^-, PO_2^- and PO_3^-, and the ion intensity ratios of C_2H^-/SiO_2^- and C_2OH^-/SiO_2^- compared with that of bare mica greatly increased from 1.7 to 11.7, and from 0.4 to 2.2, respectively. This characterization results further proved the successful deposition of poly(PO_4-DHB) coating on the mica surface.

2.4 X-ray photoelectron spectrometer (XPS) characterization

The XPS C1s spectra of PO_4-DHB and poly(PO_4-DHB) were obtained by using a Kratos Axis 165 XPS spectrophotometer (Kratos Analytical, Manchester, UK). As shown in Figure S12, compared with PO_4-DHB, in poly(PO_4-DHB), the bond percentage of C-O/C-N is lower, while the bond percentage of C=O is higher, which should be attributed to the oxidation of a portion of catechol moieties containing C-OH groups to quinone moieties containing C=O groups. As shown in Figure S15a, according to previous studies, upon exposure to air, catechol in PO_4-DHB would be spontaneously oxidized by oxygen to *o*-semiquinone radical, along with the formation of $O_2^{\cdot-}$. The generated $O_2^{\cdot-}$ would further oxidize another catechol to form *o*-semiquinone radical. The produced two *o*-semiquinone radicals can form quinone and catechol.[11-12] Thus, the transition from *o*-semiquinone radicals to catechol and quinone are reversible, during which the polymerization of PO_4-DHB can be initiated.[11] The oxidation of catechol to quinone is substantiated by XPS characterization. In the following section, the presence of *o*-semiquinone radical would be further verified by using electron paramagnetic spectroscopy (EPR).

2.5 Electron paramagnetic spectroscopy (EPR) characterization

As shown in Figure S13, the EPR spectrum of PO_4-DHB buffer solution (initial concentration of PO_4-DHB: 2 mg/mL, pH 8.4, 50 mM bicine and 150 mM KNO_3) was acquired by using a Bruker Elexys E500 spectrometer (Billerica, MA). The instrument parameters were set as follows: frequency, 9.86 GHz; microwave power, 20 mW; modulation amplitude, 1.0 G; modulation frequency, 100 kHz. The EPR signal peak of the measured free radical is located at ~3314 G with g-value of 2.005, corresponding to typical *o*-semiquinone radical.[13-14]

2.6 UV-vis adsorption analysis

The time-dependent UV-vis adsorption spectra of PO_4-DHB (initial concentration: 2 mg/mL) in bicine buffer solution (pH 8.4, 150 mM KNO_3) are shown in Figure S14. It can be observed that the adsorption of a broad range of wavelength (~380 nm to ~700 nm) increases with time. The increased adsorption at ~400 nm should be attributed to the oxidation of catechol in PO_4-DHB to quinone.[15-16] The increased adsorption at higher wavelength up to 700 nm should be attributed to the oxidative polymerization due to the occurred *o*-semiquinone radical.[15-16] The broad wavelength adsorption range can be attributed to the complex polymerization routes.[15] Previously, tremendous efforts have been devoted to investigating the oxidative polymerization of catechol and its derivatives, and it is generally accepted that the polymerization route is initiated by the oxidation of catechol to quinone with occurred *o*-semiquinone radical, and the resulted products are consisted of crosslinked catechol and quinone moieties.[11, 17-18] However, due to the versatile and complex chemistry of catechol and its derivatives, their precise polymerization

routes and exact chemical structures are still not completely clear.[11, 15] Based on our characterization results and previous studies, the possible polymerization route and structure of poly(PO_4-DHB) are proposed (Figure S15b).[19-20] Upon spontaneous oxidation, the polymerization of PO_4-DHB between quinone and catechol moieties can be initiated, through C-C bonding between phenyl rings or C-O bonding between phenyl ring and deprotonated hydroxyl group. During the polymerization of PO_4-DHB, the oxidation of catechol to quinone through the intermediate *o*-semiquinone radical can occur simultaneously. Thus, the π-conjugated moieties in the resulted poly(PO_4-DHB) should include crosslinked catechol and quinone moieties, with intermediate *o*-semiquinone radical, which is substantiated by our results based on XPS, EPR and UV-vis characterizations.

Table S1. Binding energies between methyl phosphate and CMA/QMA/QRMA-K^+ pairs.

Name	Binding energy (kJ/mol)
Methyl phosphate/CMA-K^+	-58.67
Methyl phosphate/QMA-K^+	-63.62
Methyl phosphate/QRMA-K^+	-34.92

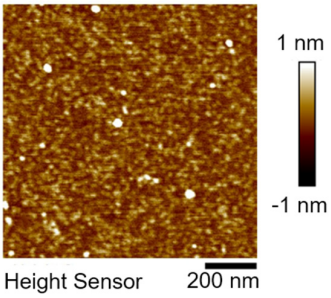

Figure S1. Atomic force microscopy (AFM) topographic image of poly(PO_4-DHB) coating.

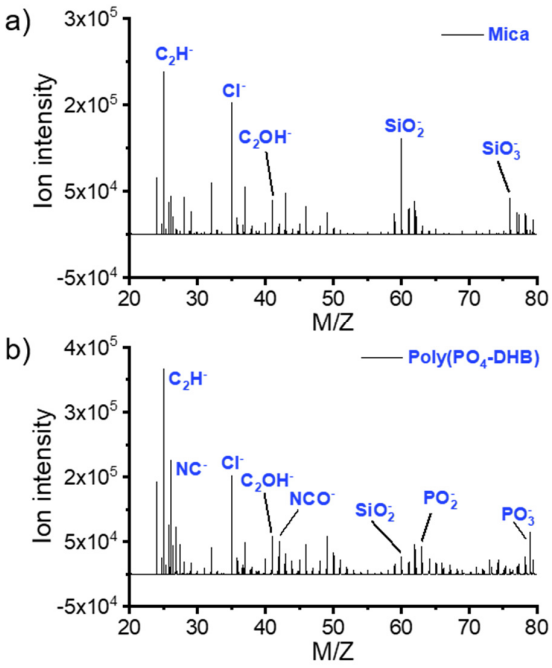

Figure S2. Negative time-of-flight secondary ion mass spectrometry (ToF-SIMS) spectra of (a) mica surface and (b) poly(PO_4-DHB) coated mica surface in m/z 20–80.

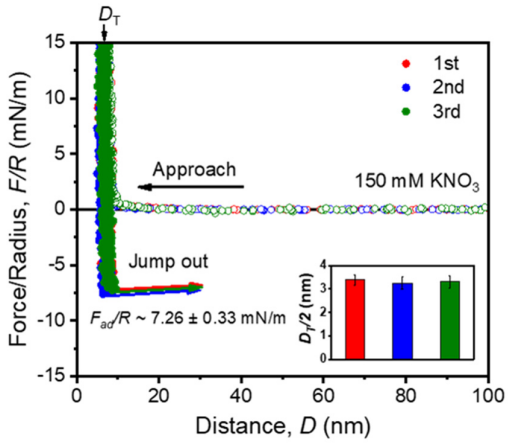

Figure S3. Force-distance profiles obtained from three sequential force measurements between two poly(PO_4-DHB) coatings with 1 hr deposition.

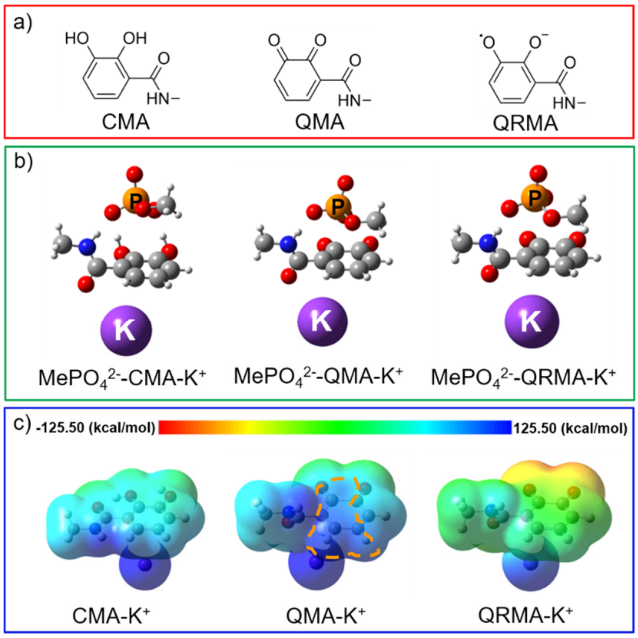

Figure S4. a) Chemical structures of methyl amides of catechol (CMA), quinone (QMA) and *o*-semiquinone radical (QRMA). b) Optimized geometries of $MePO_4^{2-}$-CMA/QMA/QRMA-K^+ complexes. The white, grey, red, navy, purple and orange balls stand for hydrogen, carbon, oxygen, nitrogen, potassium and phosphorus atoms, respective. c) Electrostatic potential (ESP) surfaces of CMA/QMA/QRMA-K^+ pairs. Orange circle marks the region with higher positive ESP on the surface of π-conjugated rings.

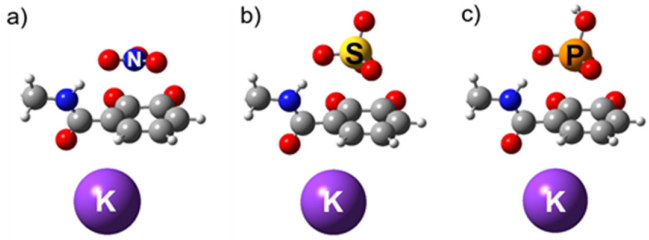

Figure S5. Optimized geometries of NO_3^-/SO_4^{2-}/HPO_4^{2-}-QMA-K^+.

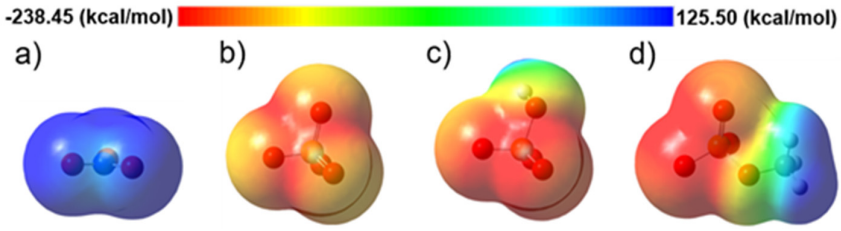

Figure S6. ESP surfaces of a) NO_3^-, b) SO_4^{2-}, c) HPO_4^{2-} and d) $MePO_4^{2-}$.

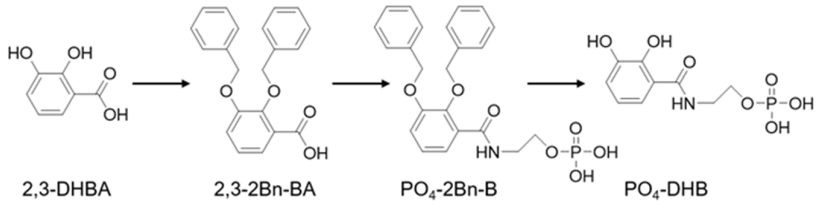

Figure S7. Synthesis scheme of PO_4-DHB.

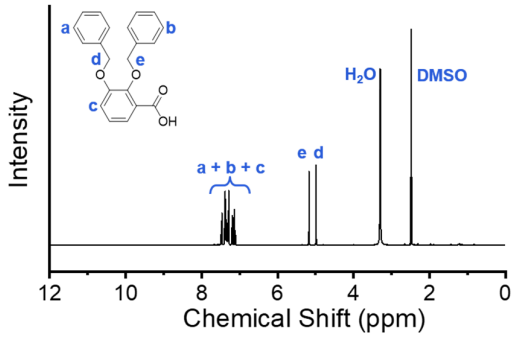

Figure S8. 1H NMR spectrum of 2,3-dibenzyloxy-benzoic acid (2,3-2Bn-BA).

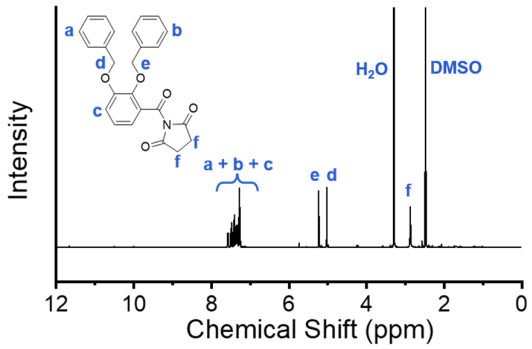

Figure S9. 1H NMR spectrum of 2,3-dibenzyloxy-benzoic acid NHS ester (2,3-2Bn-BA-NHS).

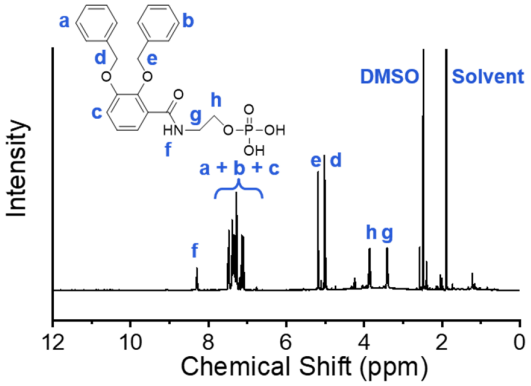

Figure S10. 1H NMR spectrum of 2-O-phosphorylethanol 2,3-dibenzyloxy-benzamide (PO_4-2Bn-B).

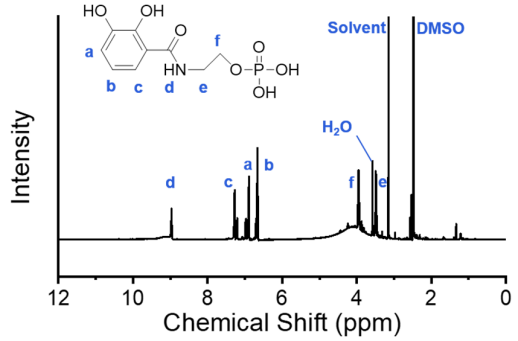

Figure S11. 1H NMR spectrum of 2-O-phosphorylethanol 2,3-hydroxybenzamide (PO_4-DHB).

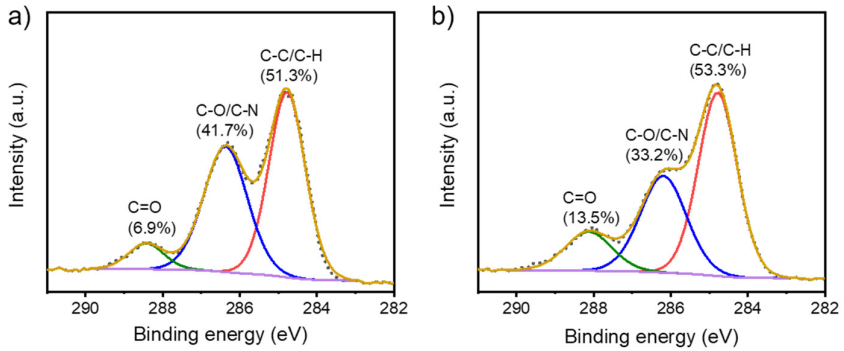

Figure S12. X-ray photoelectron spectrometer (XPS) spectra of PO_4-DHB a) before and b) after oxidative polymerization.

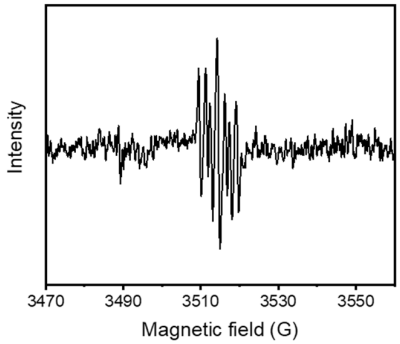

Figure S13. Electron paramagnetic spectroscopy (EPR) spectrum of PO_4-DHB solution (initial concentration of PO_4-DHB: 2 mg/mL, pH 8.4, 50 mM bicine and 150 mM KNO_3).

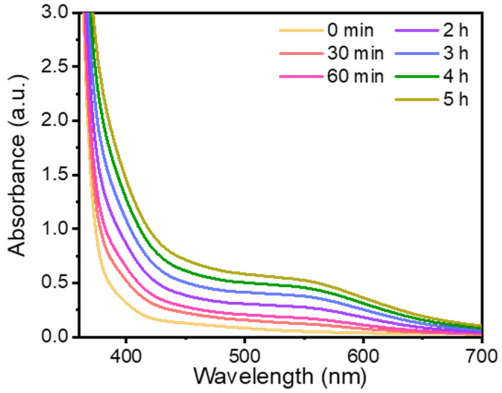

Figure S14. Time-dependent UV-vis adsorption spectra of PO_4-DHB (initial concentration: 2 mg/mL) in bicine buffer (pH 8.4, 150 mM KNO_3).

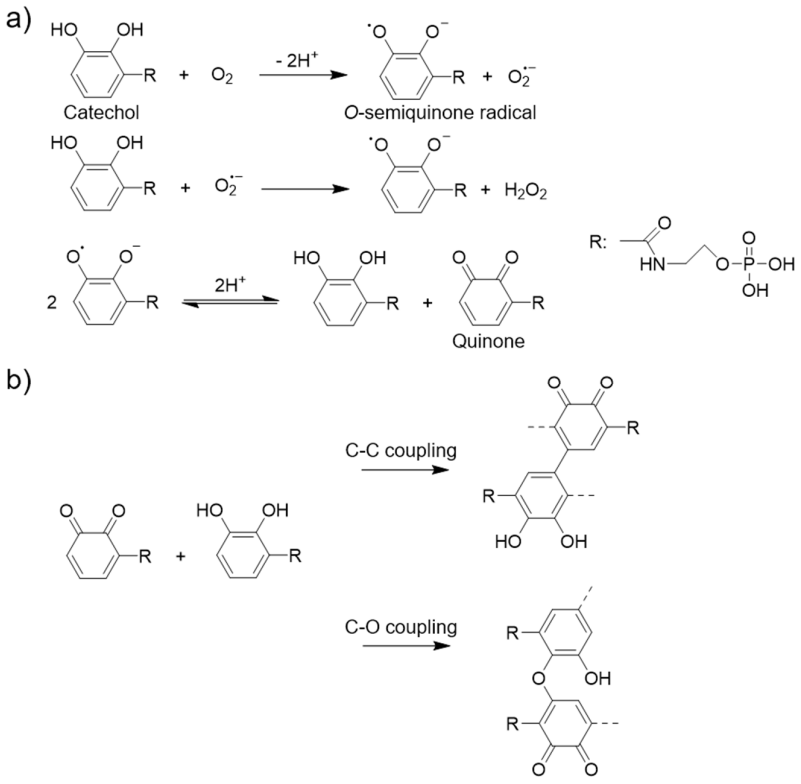

Figure S15. a) Oxidation route of catechol in PO_4-DHB to quinone, b) proposed chemical structure of poly(PO_4-DHB).

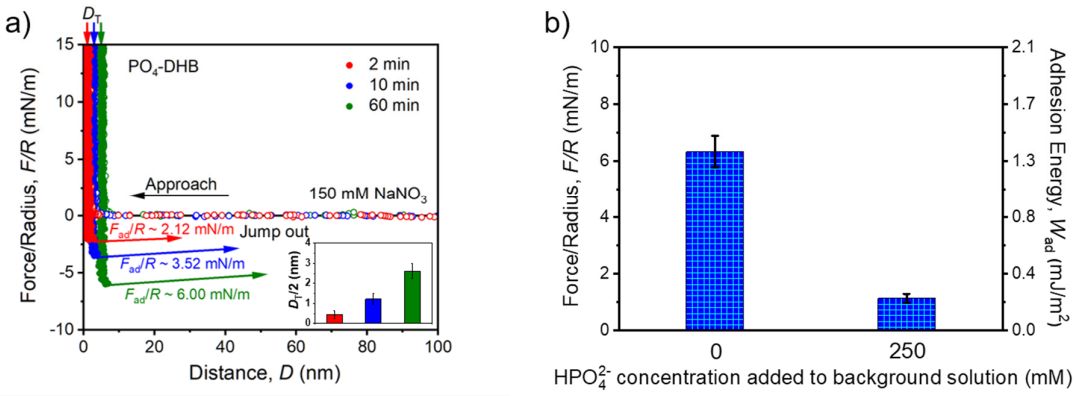

Figure S16. a) Force-distance profiles of poly(PO_4-DHB) films as function of deposition time *t* in 150 mM $NaNO_3$ buffer solution (pH 8.4, 50 mM bicine, initial concentration of PO_4-DHB: 2 mg/mL). The inset shows the thickness of each poly(PO_4-DHB) film ($D_T/2$). b) Adhesion changes between two poly(PO_4-DHB) films (1 h deposition with 150 mM $NaNO_3$) after further addition of 250 mM HPO_4^{2-} (with the concentration of corresponding counterion Na^+ as 500 mM) in 150 mM $NaNO_3$ background buffer solution.

References

1. Tse, B.; Kishi, Y., Conformationally rigid tricyclic tripods: Synthesis and application to preparation of enterobactin analogs. *J. Org. Chem.* **1994,** *59* (25), 7807-7814.

2. Bergeron, R. J.; Singh, S.; Bharti, N., Synthesis of heterobactins A and B and Nocardia heterobactin. *Tetrahedron* **2011,** *67* (18), 3163-3169.
3. Felix, A. M.; Heimer, E. P.; Lambros, T. J.; Tzougraki, C.; Meienhofer, J., Rapid removal of protecting groups from peptides by catalytic transfer hydrogenation with 1, 4-cyclohexadiene. *J. Org. Chem.* **1978,** *43* (21), 4194-4196.
4. Israelachvili, J.; Min, Y.; Akbulut, M.; Alig, A.; Carver, G.; Greene, W.; Kristiansen, K.; Meyer, E.; Pesika, N.; Rosenberg, K., Recent advances in the surface forces apparatus (SFA) technique. *Rep. Prog. Phys.* **2010,** *73* (3), 036601.
5. Zeng, H.; Kristiansen, K.; Wang, P.; Bergli, J.; Israelachvili, J., Surface-induced patterns from evaporating droplets of aqueous carbon nanotube dispersions. *Langmuir* **2011,** *27* (11), 7163-7167.
6. Faghihnejad, A.; Zeng, H., Interaction mechanism between hydrophobic and hydrophilic surfaces: Using polystyrene and mica as a model system. *Langmuir* **2013,** *29* (40), 12443-12451.
7. Israelachvili, J. N., *Intermolecular and surface forces, 3rd ed.*; Elsevier: Amsterdam, 2011.
8. Zeng, H.; Hwang, D. S.; Israelachvili, J. N.; Waite, J. H., Strong reversible Fe^{3+}-mediated bridging between dopa-containing protein films in water. *Proc. Natl. Acad. Sci. U. S. A.* **2010,** *107* (29), 12850-12853.
9. Frisch, M.; Trucks, G.; Schlegel, H.; Scuseria, G.; Robb, M.; Cheeseman, J.; Scalmani, G.; Barone, V.; Petersson, G.; Nakatsuji, H.; Li, X.; Caricato, M.; Marenich, A.; Bloino, J.; Janesko, B.; Gomperts, R.; Mennucci, B.; Hratchian, H.; Ortiz, J.; Izmaylov, A.; Sonnenberg, J.; Williams-Young, D.; Ding, F.; Lipparini, F.; Egidi, F.; Goings, J.; Peng, B.; Petrone, A.; Henderson, T.; Ranasinghe, D.; Zakrzewski, V.; Gao, J.; Rega, N.; Zheng, G.; Liang, W.; Hada, M.; Ehara, M.; Toyota, K.; Fukuda, R.; Hasegawa, J.; Ishida, M.; Nakajima, T.; Honda, Y.; Kitao, O.; Nakai, H.; Vreven, T.; Throssell, K.; Montgomery, J.; Peralta, J., JE; Ogliaro, F.; Bearpark, M.; Heyd, J.; Brothers, E.; Kudin, K.; Staroverov, V.; Keith, T.; Kobayashi, R.; Normand, J.; Raghavachari, K.; Rendell, A.; Burant, J.; Iyengar, S.; Tomasi, J.; Cossi, M.; Millam, J.; Klene, M.; Adamo, C.; Cammi, R.; Ochterski, J.; Martin, R.; Morokuma, K.; Farkas, O.; Foresman, J.; Fox, D., *Gaussian 09, Revision E. 01, Gaussian, Inc., Wallingford CT* **2016**.
10. Grimme, S.; Ehrlich, S.; Goerigk, L., Effect of the damping function in dispersion corrected density functional theory. *J. Comput. Chem.* **2011,** *32* (7), 1456-1465.
11. Yang, J.; Stuart, M. A. C.; Kamperman, M., Jack of all trades: versatile catechol crosslinking mechanisms. *Chem. Soc. Rev.* **2014,** *43* (24), 8271-8298.
12. Kalyanaraman, B.; Felix, C.; Sealy, R., Semiquinone anion radicals of catechol(amine)s, catechol estrogens, and their metal ion complexes. *Environ. Health Perspect.* **1985,** *64*, 185-198.
13. Wu, T.-L.; Qin, W.-X.; Alves, M. E.; Fang, G.-D.; Sun, Q.; Cui, P.-X.; Liu, C.; Zhou, D.-M.; Wang, Y.-J., Mechanisms of Sb (III) oxidation mediated by low molecular weight phenolic acids. *Chem. Eng. J.* **2019,** *356*, 190-198.
14. Saab, S. C.; Martin-Neto, L., Characterization by electron paramagnetic resonance of organic matter in whole soil (Gleysoil) and organic-mineral fractions. *J. Braz. Chem. Soc.* **2008,** *19* (3), 413-417.
15. Hong, S.; Wang, Y.; Park, S. Y.; Lee, H., Progressive fuzzy cation-π assembly of biological catecholamines. *Sci. Adv.* **2018,** *4* (9), eaat7457.

16. Burzio, L. A.; Waite, J. H., Cross-linking in adhesive quinoproteins: studies with model decapeptides. *Biochemistry* **2000,** *39* (36), 11147-11153.
17. Lim, C.; Huang, J.; Kim, S.; Lee, H.; Zeng, H.; Hwang, D. S., Nanomechanics of poly(catecholamine) coatings in aqueous solutions. *Angew. Chem. Int. Ed.* **2016,** *55* (10), 3342-3346.
18. Moulay, S., Dopa/catechol-tethered polymers: Bioadhesives and biomimetic adhesive materials. *Polym. Rev.* **2014,** *54* (3), 436-513.
19. Hong, S.; Lee, H.; Lee, H., Controlling mechanical properties of bio-inspired hydrogels by modulating nano-scale, inter-polymeric junctions. *Beilstein J. Nanotechnol.* **2014,** *5* (1), 887-894.
20. Sanchez-Cortes, S.; Francioso, O.; Garcıa-Ramos, J.; Ciavatta, C.; Gessa, C., Catechol polymerization in the presence of silver surface. *Colloids Surf. Physicochem. Eng. Aspects* **2001,** *176* (2-3), 177-184.